Exp. in Fluids manuscript No.
(will be inserted by the editor)

Highly spatially resolving laser Doppler velocity measurements of the tip clearance flow inside a hard disk drive model

Katsuaki Shirai · Yusuke Yaguchi · Lars Büttner · Jürgen Czarske · Shinnosuke Obi

Received: date / Accepted: date

Abstract The flow in the tip clearance of a hard disk drive model has been investigated with laser Doppler techniques. The flow was driven by co-rotating disks inside a cylindrical enclosure in order to simulate a hard disk drive used for data storage devices. The main focus of the investigation was on the understanding of complex flow behavior in the narrow gap region between the disk tip and the outer shroud wall, which is supposed to be one of the causes of flow induced vibration of the disks. Experiments in the past have never been able to examine this region because of the lack of the spatial resolution of sensors in the highly three dimensional flow in the region. In the present investigation, the flow velocity in the tip clearance region was measured with optical measurement techniques for the first time. The flow behaviors are investigated for four different conditions with two different gap widths and two different shapes of the shroud walls with and without ribs. The velocity measurements were carried out both with conventional laser Doppler velocimetry and using a laser Doppler velocity profile sensor with a spatial resolution in the micrometer range. The circumferential velocity component was measured along the axial and radial directions. The steep gradients of the circumferential mean velocity in both directions were successfully captured with a high spatial resolution, which was achieved by the velocity profile sensor. From the supplementary investigations, the existence of vortex structures in the tip clearance region was confirmed with a dependence on the shroud gap width and the shroud shape. The interactions of the two boundary layers seem to be the source of the complex three dimensional behaviors of the flow in this region.

Keywords hard disk drive · laser Doppler velocimetry · velocity profile sensor · spatial averaging effect · tip clearance flow · secondary flow

Y. Yaguchi · S. Obi
Department of Mechanical Engineering, Keio University
3–14–1 Hiyoshi, Kouhoku–ku, Yokohama 223–8522, Japan
Tel.: +81-45-566-1499
Fax.: +81-45-566-1495
E-mail: obsn@mech.keio.ac.jp

K. Shirai · L. Büttner · J. Czarske
Faculty of Electrical Engineering and Information Technology, Laboratory for Measurement and Testing Techniques, Technische Universität Dresden (TU Dresden),
Helmholtzstraße 18, 01069, Dresden, Germany
Tel.: +49-351-463-36192
Fax.: +49-351-463-37716
E-mail: katsuaki.shirai@tu-dresden.de

Nomenclature

c	Tip clearance
d	Fringe spacing of the LDV
d_1, d_2	Fringe spacings of the velocity profile sensor
f	Doppler frequency of the LDV
f_1, f_2	Doppler frequencies of the profile sensor
H	Center-to-center distance between two disks
r_c^*	Radial coordinate normalized by tip clearance ($r_c^* = r_c/c$)
r_d	Radial coordinate originating from the spindle periphery
R_1, R_2, R_3	Radius of spacer, disk and shroud
Re_D	Disk Reynolds number ($Re_D = {R_2}^2\Omega/\nu$)
t_d, t_s	Thickness of disk and spacer
q	Quotient of two Doppler frequencies ($q = f_1/f_2$)
v	Velocity of a tracer particle
${V_\theta}^*$, ${V_r}^*$	Normalized tangential and radial velocity components (${V_\theta}^* = V_\theta/\Omega R_2$, ${V_r}^* = V_r/\Omega R_2$)
$\overline{{v_\theta}^2}^*$, $\overline{{v_r}^2}^*$	Normal components of the Reynolds stress ($\overline{{v_\theta}^2}^* = \overline{{v_\theta}^2}/(\Omega R_2)^2$, $\overline{{v_r}^2}^* = \overline{{v_r}^2}/(\Omega R_2)^2$)
z	Optical axis
z^*	Axial coordinate normalized by the disk spacing ($z^* = z/H$)

Greek symbols

ν	Kinematic viscosity
$\sigma_f, \sigma_v, \sigma_z$	Uncertainty of measured frequency, velocity and position
Ω	Rotational speed

Superscripts

$\bar{\cdot}$	Time averaged value
$\hat{\cdot}$	Instantaneous value

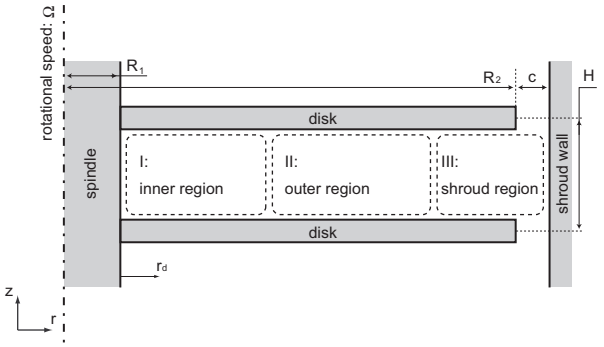

Fig. 1 Sketch of the flow regions in a co-rotating disk system. Region I is the "inner region" where the flow exhibits solid body rotation. Region II is the "outer region" where the distinct vortical structure is formed. Region III is the "shroud region" where significant turbulence production occurs due to strong shear with the shroud wall.

1 Introduction

Hard disk drives (HDDs) are among the most widely spread data storage devices. With the continuously growing demand for larger storage capacity and faster data access speed, the development of HDDs is tending toward higher data densities with faster rotation speeds. On the other hand, the next generation of HDDs is expected to be smaller in size and to consume less energy. Currently 3.5-in HDDs capable of speeds of up to 15,000 rpm are commercially available. The gap between the read-and-write head and the disk surface reaches into the range of 10 nm for the most recently developed products. As a consequence, vibration of the disks is gaining more importance in the development of new HDDs. Due to the fast rotation of the disks, surrounding air is entrained, causing three-dimensional complex flow structures develop around the disks (Abrahamson et al. 1989; Humphrey and Gor 1993). The detailed mechanism of the flow-disk-interaction is currently not completely understood.

Basically, several different flow regimes are commonly observed in the flow in a co-rotating disk system. As presented in Fig. 1, the flow regimes can roughly be categorized into three different regions: inner, outer and shroud regions whereas Schuler et al. (1990) identified five different characteristic regions and Wu (2009) classified the flow into three different regions. Region I ($0 \leq r_d/R_2 \leq 0.4$) is the "inner region" where flow exhibits the solid body rotation. Here, r_d is the radial coordinate originating from the exterior of the spindle and R_2 stands for the radius of the disk. Region II ($0.4 \leq r_d/R_2 \leq 0.75$) is the "outer region" where distinct vortical structure can be observed. Region III ($r_d/R_2 \geq 0.75$) is the "shroud region" where significant turbulent production occurs due to strong shear with the shroud wall. In the present study, we focus on the region of tip clearance which is a part of region III. In this region, however, the flow quantities show a significant gradient in both the axial and radial directions due to the existence of strong shear in both directions.

The behaviors and mechanisms of disk vibration have been investigated by many researchers using capacitive sensors (Fukaya et al. 2002), laser triangulation (Kang and Ramen 2006) and laser Doppler vibrometry (Takeda et al. 2007; Pang et al. 2008). The flow behaviors in a HDD have also been investigated into a certain extent using experiments (Abrahamson et al. 1989; Humphrey and Gor 1993; Fukaya et al. 2002; Schuler et al. 1990; Kanagai et al. 2007; Wu 2009) and numerical simulations (Suzuki and Humphrey 1997; Tatewaki et al. 2001; Al-Shannag et al. 2002; Kirpekar and Bogy 2008). In experimental investigations, flow visualizations (Humphrey and Gor 1993), laser Doppler velocimetry (LDV) (Schuler et al. 1990), hot-wire anemometry (HWA) (Fukaya et al. 2002; Kanagai et al. 2007) and particle image velocimetry (PIV) (Kanagai et al. 2007; Wu 2009) have been applied. However, these investigations focused on the flow inside the large region between the disks and no investigations have ever focused on the flow in the narrow tip clearance region between the disk and the outer shroud. Based on a numerical analysis Suzuki and Humphrey (1997) showed first that out-of-phase pressure fluctuations arise on either side of a disk rotating in an enclosure. The results of the large eddy simulation (LES) performed by Tatewaki et al. (2001) have revealed the existence of spatial surface pressure patterns with a phase difference between the top and the bottom surface of a disk. They suspected that the pressure patterns with phase difference are the cause of the disk flutter. Then, the question is the origin of the wall-pressure patterns and their connections to the flow behaviors. In this point, Kirpekar and Bogy (2008) have performed an LES and pointed out the velocity fluctuations in the shroud gap correlate very well with the pressure fluctuations.

In order to answer this question, detailed flow behavior has to be investigated, especially with respect to the possibility of inter-disk exchange of momentum through the narrow tip clearance region. It has been known that the disk vibration decreases either by narrowing the tip clearance between

the disk and the shroud (Imai et al. 1999; Imai 2001) or by using a shroud wall with a ribbed shape (Yamamoto et al. 2004). The reduction mechanism of the disk vibration needs to be clarified and the investigation of the flow inside the tip clearance region is of greatest interest. However, investigation of the flow behavior in this region remains very difficult for two major reasons: First of all, experimental investigations using a full size model are difficult due to the very thin dimensions of the tip clearance, which are smaller than 500 μm for a commercial 3.5-in HDD. Secondly, the flow inside the gap should exhibit highly three dimensional structures due to the mean shear forces induced along two axes, namely, the axial and the radial directions accompanying the disk rotation. Therefore, a sophisticated measurement technique is required so as not to disturb the flow while simultaneously achieving high spatial resolution. None of the conventional measurement techniques afford these requirements. Probes, such as HWA, would disturb the flow and the spatial resolution of sensors is the critical issue. Application of PIV is also very difficult since the area of interest is very small with high shear rate in two directions.

The use of a novel laser Doppler velocity profile sensor is considered in order to overcome the aforementioned difficulty. This sensor was developed by Czarske (2001); Czarske et al. (2002) as an extension of the conventional LDV technique. In contrast to conventional LDV which uses a single interference fringe system with almost parallel spacing (see Fig. 2(a)), the profile sensor employs a pair of fan-like fringe systems superposed in a single measurement volume consisting of diverging and converging spacings along the optical axis (see Fig. 2(b)). This allows the determination of not only the lateral velocities but also the axial positions of single tracer particles inside the measurement volume. The sensor has several substantial advantages over the conventional LDV, e.g., a sub-micrometer spatial resolution (Büttner et al. 2005) and a small measurement uncertainty of velocities (Büttner et al. 2008). Actual spatial resolution has been demonstrated to be better than 960 nm, confirmed in a real flow measurement using a micro channel with one of the sensors (König et al. 2010). Furthermore, the sensor systems have been successfully applied to the investigation of the near-wall behaviors of turbulence statistics in a fully developed channel flow (Shirai et al. 2008) and metrological development of the precise flow rate measurement technique (Büttner et al. 2008).

In this paper, we report on the velocity measurement of fluid flow in the narrow gap region between the disk and the shroud of a scaled experimental model of a HDD. The measurements were carried out both with a conventional LDV and with a laser Doppler velocity profile sensor. Our main focus is on the complex flow behaviors in the tip clearance region where the steep velocity gradient and significant velocity fluctuations would take place. Further attention was paid to the variation of the secondary flow patterns due to the different gap widths and geometrical configurations of the shroud walls with and without ribs.

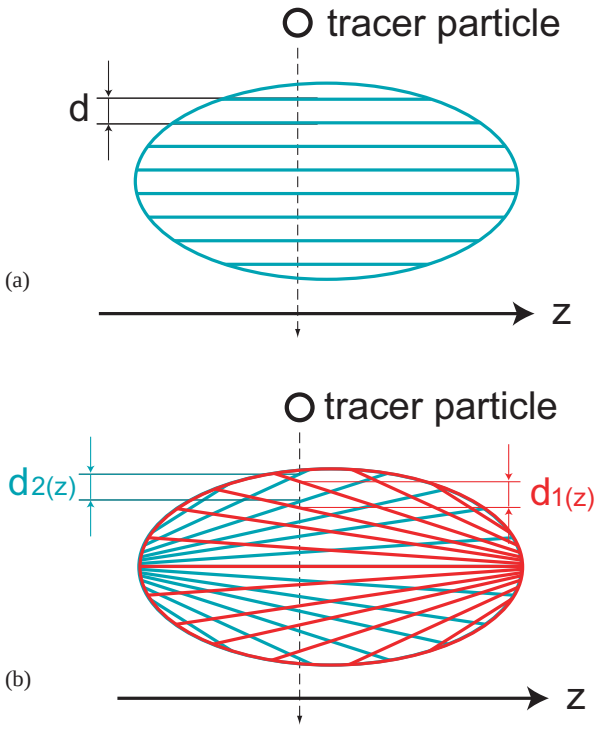

Fig. 2 Schematic comparison of the fringe systems of (a) a conventional LDV and (b) a laser Doppler velocity profile sensor. The velocity profile sensor utilizes a pair of fringe systems with fan-like shapes along the optical axis z, while a conventional LDV uses a nominally parallel fringe system. The two fringe systems of the velocity profile sensor allow the determination of the velocities and axial positions of single tracer particles inside the measurement volume.

2 Laser Doppler Velocity Profile Sensor

2.1 Principle of velocity profile senor

The laser Doppler velocity profile sensor has been developed as an extension of the conventional LDV. The profile sensor measures both the lateral velocities and the axial path positions of single tracer particles inside the measurement volume. The local flow velocity can be measured as long as the tracer particles follow the local motions of the fluid without slipping. The fundamental principles and uncertainties have been investigated and described in detail in former publications (Czarske 2001; Czarske et al. 2002; Bayer et al. 2008).

Fig. 2 shows a schematic comparison of the interference fringe patterns used in a conventional LDV (see Fig. 2(a)) and in the velocity profile sensor (see Fig. 2(b)). The coordinates are taken so that z is the direction of the optical axis

and v is the velocity perpendicular to the bisector plane of the laser beams assuming that the optical axis is contained in the beam bisector plane. The LDV uses the parallel fringe system as shown in Fig. 2(a), while the laser Doppler velocity profile sensor uses a pair of fan-like fringe systems as shown in Fig. 2(b).

The velocity of a tracer particle v for the case of a conventional LDV is determined by the product of the Doppler frequency f and the fringe spacings d, provided that the fringe spacing is determined either by geometrical relation or by calibration. In the case of the velocity profile sensor, it gives a pair of the Doppler frequencies, f_1 and f_2, from each interference fringe system. When the fringe spacings depend on z, the particle velocity can be described as

$$v = f_1(v,z)d_1(z) = f_2(v,z)d_2(z). \tag{1}$$

The quotient of two Doppler frequencies, q, is equal to the ratio of two fringe spacings:

$$q(z) = \frac{f_1(v,z)}{f_2(v,z)} = \frac{d_2(z)}{d_1(z)}. \tag{2}$$

From this equation, it turns out that q is dependent only on the axial position z and not on the velocity. Therefore, once the relationship of q and z is determined, the path position of a single particle passing through the measurement volume can be determined from the measured Doppler frequency pair. The $q-z$ curve can be obtained by a calibration of $d_1(z)$ and $d_2(z)$ prior to flow measurement. In order to distinguish the two fringe systems, one can use either different wavelengths (wavelength division multiplexing: WDM) (Büttner et al. 2005), different frequency ranges (frequency division multiplexing: FDM) (Büttner et al. 2008; Pfister et al. 2005), or different timing of pulse sequences (time division multiplexing: TDM) (König et al. 2010). In the present investigation, an FDM technique was utilized for realizing the velocity profile sensor. From the measured position-velocity data of many particles distributed in the flow, the velocity profile inside the measurement volume is reproduced with a much higher resolution than the measurement volume size without traversing the probe.

2.2 Uncertainty analysis

Velocity measurement uncertainties are considered for conventional LDV and for the velocity profile sensor. The uncertainty considered here is the intrinsically existing one in the sensors, while statistical one depends on the number of statistically independent samples in experiments. The measurement uncertainty of velocity for a conventional LDV is mainly determined by the non-uniform fringe spacings along the optical axis. The nominally parallel fringe systems of a conventional LDV have a maximum fringe spacing variation of approximately 1 % along the optical axis due to the nature of Gaussian laser beams (Miles 1996). Hence, the systematic measurement uncertainty for the flow velocity stays around 0.6 % even for a perfectly aligned LDV. The measurement uncertainty of the velocity profile sensor was derived by Czarske et al. (2002)

$$\frac{\sigma_v}{v} \approx \sqrt{\frac{3}{2}}\frac{\sigma_f}{f}. \tag{3}$$

Unlike the conventional LDV, the uncertainties of the velocities measured with the profile sensor ideally depend only on the estimate uncertainties of the Doppler frequencies which depend on the signal-to-noise ratio (SNR). This is due to the fact that the variation of the local fringe spacings is taken into account by the calibration in the case of the velocity profile sensor. The uncertainty of the position estimate, which is equivalent to the spatial resolution, is given by (Czarske et al. 2002)

$$\sigma_z \approx \sqrt{2}\left|\frac{\partial q(z)}{\partial z}\right|^{-1}\frac{\sigma_f}{f}. \tag{4}$$

Thus, the spatial resolution of the profile sensor is determined by the slope of the calibration curve $|\partial q(z)/\partial z|$ and the error in the estimation of the Doppler frequencies. An extensive analysis of the spatial resolution based on the theory of Cramer-Rao's lower bound (CRLB) with SNR was developed by Bayer et al. (2008).

3 Experiments

3.1 Flow apparatus

A simplified experimental scale model of a HDD was constructed for the present investigation as shown in Fig. 3. It was scaled up approximately 3.4 times from the commonly used 3.5-in HDD. Five polymethyl-methacrylate (PMMA) disks of thickness 3 mm were equidistantly placed using acrylonitrile butadiene styrene (ABS) spacers of the radius 50 mm and thickness 9 mm. The disks and spacers were fixed to a shaft and put inside a cylindrical PMMA enclosure casing (shroud) of inner-wall radius 155 mm. The enclosure was filled with normal tap water which served as working fluid. The shaft was directly connected to the rotating shaft of a brushless DC motor (3IK15GN-AW2, Oriental Motor Co. Ltd., Tokyo) through the bottom wall of the casing. The rotation of the motor was controlled to within a stability of ±0.2 % according to the specification. The disks and the spacers were variable while the inner-wall diameter of the outer casing was set fixed. Two sets of the disks with different radii were used in order to realize different widths of the tip clearance, c=5 mm and 2 mm, respectively. These tip clearances corresponded to 1.5 mm and 0.6 mm for the 3.5-in HDD, and the latter is equivalent to the clearance of a commercially available HDD. The rotation speed

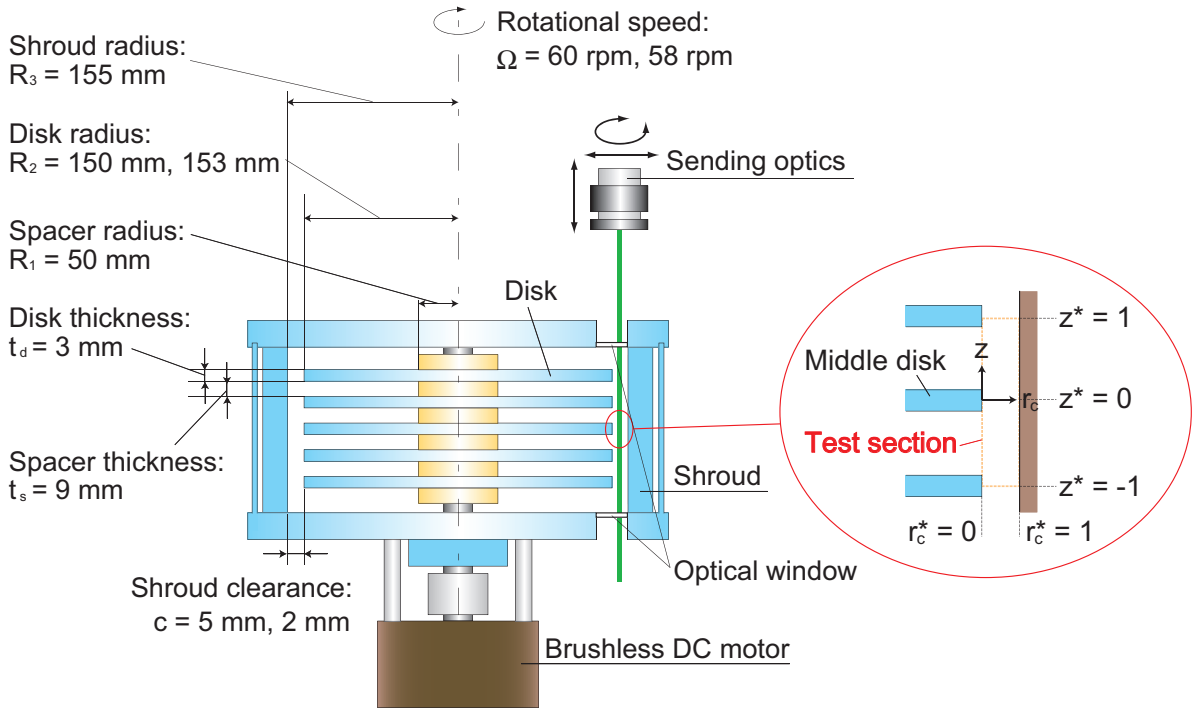

Fig. 3 Schematic of the simplified experimental model of a HDD. The disks are rotated by the DC motor and the enclosure was filled with water. Two flush-mounted optical ports were equipped at the top and the bottom of the model. The disks and shrouds were exchangeable so that the gap width of the tip clearance and the shroud shape could be changed.

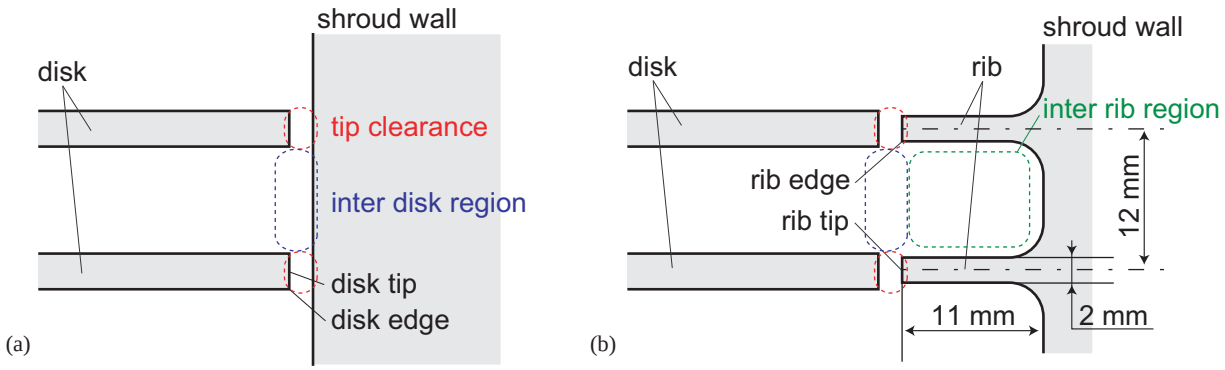

Fig. 4 Two different configurations of the shroud shapes investigated: (a) flat-shaped shroud, (b) ribbed-shape shroud.

was adjusted for the two different sets of the disks so that the resulting disk Reynolds number remained constant for all of our investigations. The disk Reynolds number was based on the angular velocity Ω, the disk radius R_2 and the kinematic viscosity of water ν, $Re_D=R_2^2\Omega/\nu$, which was set to 1.4×10^5 corresponding to 10,000 rpm in a real 3.5-in HDD. The shroud was exchangeable so that different peripheral shapes of the shroud could be tested at each respective gap width. Two different types of shroud shapes termed “flat” and “ribbed” were prepared as depicted in Fig. 4. The flat shroud had a smooth inner surface and the ribbed shroud had five ribs each of thickness 2 mm. Beside the ribs, grooves with 11 mm deep were carved outward from the rib surface $r_c^*=1$. The ribs were placed at the same vertical position aligned to the corresponding disk at their middle planes (see Fig. 4). Optical windows with anti-reflection coating were placed flush with the inner surface of the top and the bottom of the casing for optical access.

We configured the test section in the region near the tip clearance as shown in Fig. 3. The measurements were undertaken in the r_c–z plane with the r_c– and z–axes originating from the middle of the third disk tip. The positions are normalized by the tip clearance and the center-to-center distance between two disks, respectively. r_c^* is the normalized radial position such that $r_c^*=0$ refers to the outermost position of the disk (disk tip) and $r_c^*=1$ refers to the position of the inner shroud wall for the flat shroud case or the innermost position of the rib for the ribbed shroud case. z^* is the

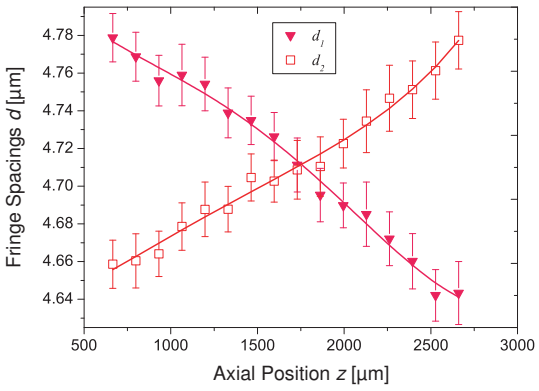

Fig. 5 Fringe spacing curves for the two fringe systems of the FDM velocity profile sensor used in the measurement. The error bars correponds to the uncertainties. The two fringe systems were set so that one has diverging and the other has converging fringe spacings in the direction of the optical axis. The points are from the calibration experiment and the solid lines are polynomial fits.

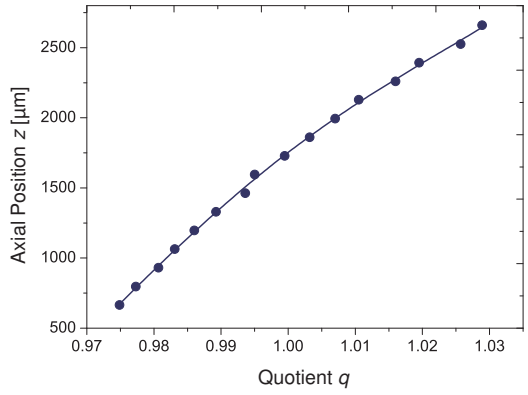

Fig. 6 The calibration curve obtained from Fig. 5. The points are from the calibration experiment and the solid lines are fit curves.

normalized axial position such that z^*=0 refers to the central plane of one disk and z^*=1 refers to the center of the overlying disk. $V_\theta{}^*(= V_\theta/\Omega R_2)$ and $V_r{}^*(= V_r/\Omega R_2)$ are the circumferential (tangential) and the radial velocity components, respectively, normalized with the circumferential velocity of the disk (Ω is the angular velocity of the disk and R_2 is the disk diameter). As presented in Fig. 4, we refer to different regions of flow in the test section as "tip clearance", "inter disk region" and "inter rib region". All measurements presented in this paper were obtained in the area around the third disk located at the middle in accordance with the preceding related studies(Yamamoto et al. 2004; Kanagai et al. 2007).

This simplified model does not necessarily represent the state-of-the-art of the commercial HDD configuration. For example, the ratio between the clearance and disk radius, i.e., $c/R_2 = 0.0133$, is larger compared with the case of high-performance server HDD. In addition, the use of ribbed shroud wall was once considered as a possible measure to reduce the flow induced vibration of the disks; however minimizing the disk clearance itself is found to be more cost-effective in the latest HDD design. The present configurations are nevertheless chosen to understand the fundamental physics and to serve as the benchmark of CFD studies. The measurements in more realistic HDD models are within the scope of our future study.

3.2 Laser Doppler sensors

Two different types of laser Doppler sensors were used in the present investigation. We used a conventional LDV and a velocity profile sensor. A commercial fiber-optic one-component LDV system (LV5000, Ono Sokki Co. Ltd., Yokohama) was used. The laser source was an air-cooled Ar-ion Laser with a 100 mW output (5500A, Ion Laser Technology Inc., UT). The fiber-optic measurement head has a working distance of 250 mm. The estimated dimensions of the measurement volume were 83.8 μm and 1.6 mm in diameter and length in water, respectively. A hardware based signal processor (Burst Correlator LV-5900, Ono Sokki Co. Ltd., Yokohama) was used for processing the burst signals in the single-burst mode.

The velocity profile sensor used in the present study was based on a FDM technique which distinguished the two fringe systems with two different carrier frequencies. The present FDM sensor was almost identical to the one used for a metrological application (Büttner et al. 2008). The details of the FDM sensor system were described in Pfister et al. (2005). The fiber-optic measurement head (Büttner et al. 2008) has a working distance of about 560 mm. The dimensions of the measurement volume were approximately 200 μm and 2000 μm in diameter and length in water, respectively. The sensor was attached to a three-axis linear precision stage for adjustment and traversing of the measurement volume. The position of the measurement volume was manually shifted and the axial position z was monitored at all the times with a laser triangulation sensor with a resolution of 0.5 μm (optoNCDT 1700-10, Micro-Epsilon Messtechnik GmbH & Co. KG, Ortenburg). The circumferential component of the flow velocity was measured in the gap region. The sensor was calibrated in-situ using a small pinhole attached to a specially-made calibration disk which was exchangeable with the third disk. The calibration was performed at the same rotational speed of the disks for the flow measurement underwater. The fringe spacings and the calibration curve are shown in Figs. 5 and 6. From the calibration data, the spatial resolution of the sensor was estimated to be approximately 22 μm along the z axis in water. The resulting theoretical uncertainty of the velocity measurements was 0.04 %. These esti-

Table 1 Measurement conditions.

Case	tip clearance [mm]	shroud wall type
F5	5	flat
F2	2	flat
R5	5	ribbed
R2	2	ribbed

mates were derived from the SNR of the signals in the calibration (Bayer et al. 2008).

3.3 Measurement Conditions

We have tested four different configurations of the disks and shroud shapes comprising combinations of flat or ribbed shroud shapes and gap widths of 5 mm or 2 mm. Hereafter, these different cases are denoted by the names of the cases: F5, F2, R5 and R2 as summarized in Table 1.

For the velocity measurements with the conventional LDV, forward-scattered signals were detected in the backward direction using a retroreflector placed at the opposite side of the test rig in order to enhance the signal quality detected in the backscattered direction. Naturally occurring dust in the water functioned as tracer particles, therefore tracer particles were not added for the LDV measurement. At each measurement location, at least 5000 samples were acquired for calculating turbulent statistics. Velocity bias was corrected based on transit-time weighting (Edwards 1987) of the burst signals for statistical calculations. The data rate was approximately 20–80 Hz depending on the measurement locations. The measurement probe of the LDV was traversed in the r and z directions using linear precision stages with a resolution of ±20 μm controlled with a standard computer. The traverse step size was set to 1.6 mm in the z direction. This corresponds to the longitudinal size of the measurement volume, equivalent to the spatial resolution of the LDV in z direction. The traverse step in the radial direction was set to 1 mm in the cases of the 5 mm gap width in the range of $0.4 \le r_c^* \le 0.8$. In all other cases, the step size was set to every 0.2 mm in the radial direction. The traversing and data acquisition were controlled with self-made software written in LabView®.

For the measurements made with the velocity profile sensor, backward scattering was mainly used and forward-scatter detection was used only for regions inaccessible by backscatter detection. The same pinhole used for the calibration was also used for precisely adjusting the location of the measurement volume. Silver-coated hollow glass spheres with ranging 2–20 μm in diameter (mean diameter: 10 μm) were seeded as tracer particles so that sufficient modulation could be obtained in the resulting Doppler signals detected with the backscatter configuration. The measurement volume was traversed with an increment of 1.6 mm along the axial direction in water. The traverse distance of 1.6 mm is smaller than the measurement length of the sensor (=2.0 mm), which means that the resulting velocity data had an overlap of 0.4 mm for every neighboring measurement location. This was done in order to avoid discontinuity of resulting statistics due to lack of samples at the edge of the measurement volume traversed without overlapping. The traverse distance in the radial direction was set to 0.2 mm for most cases. Only for the cases of 5 mm gap width the traverse distance was set to 1 mm in the range of $0.4 \le r_c^* \le 0.8$ since changes in velocity were smaller under these conditions. From the preliminary measurements with the LDV, the axial distributions of the velocity variance was found to be almost symmetric to the middle plane of the disk ($z^*=0$) in the range of $-1 \le z^* \le 1$. In addition, the variance was found to be almost symmetric with respect to the plane of $z^*=0.5$ in the range of $0 \le z^* \le 1$. Therefore, the velocity distributions in the range of $0 \le z^* \le 0.5$ were tightly focused and hence, the velocity distributions in the test section, $0 \le r_c^* \le 1$ and $-0.2 \le z^* \le 0.7$, were measured with the velocity profile sensor. Roughly 35000 samples were collected at every location of the measurement volume. The data rate was 20–80 Hz depending on the measurement location and the seeding density. Temperature variation of the water was negligible since the rotation rate of the disk was sufficiently slow to avoid heating up the water and the entire experiment, including the calibration, was carried out in a temperature regulated laboratory with a temperature stability of ±0.5 °C for the case of the velocity profile sensor.

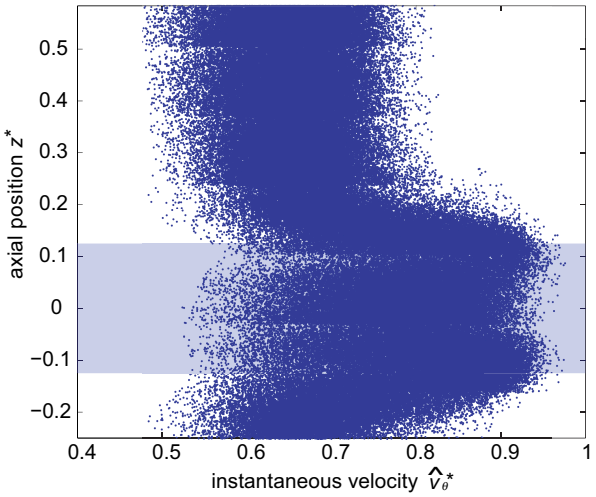

Fig. 7 Raw data of the circumferential velocity $\hat{v}_\theta^*$ measured at $r_c^* = 0.12$ with the velocity profile sensor. Total number of samples plotted in the figure is 245000. The individual point represents single contributions from single tracer particles. The disk position is indicated by the shaded area.

In Fig. 7, the raw data of the instantaneous circumferential velocity $V_\theta{}^*$ at $r_c^*=0.12$ are plotted for case F5. The position of the third disk is indicated by the shaded area. The measurements were performed at seven different locations

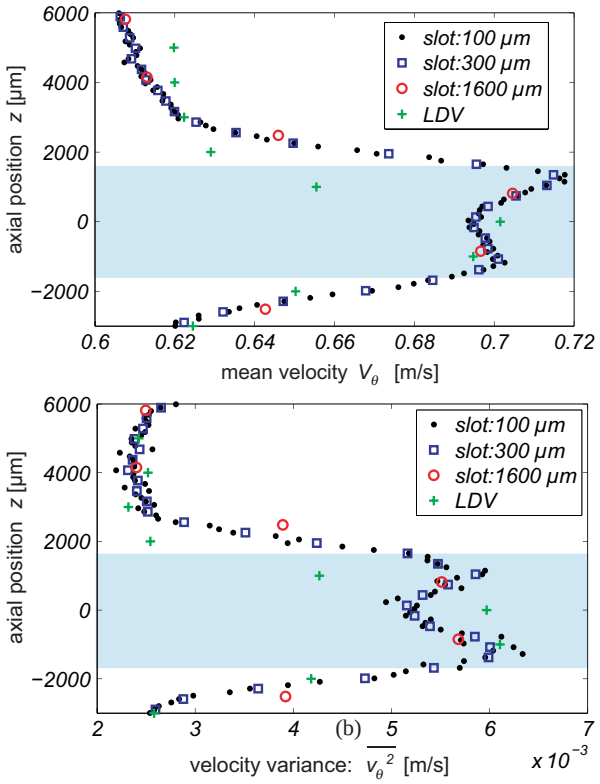

Fig. 8 Effect of the slot width on the resulting statistics: (a) mean velocity; (b) velocity variance. The statistics were calculated from the raw data displayed in Fig. 7 and shown on a real scale without nondimensionalization. The LDV results are also plotted as a reference. The disk position is indicated by the shaded area.

and 245000 samples were obtained in total. The individual points plotted in this figure represent contributions from single tracer particles. The raw data provides a rough overview of the velocity behavior in the region.

3.4 Determination of spatial resolution

In order to see the statistical behavior of the flow velocity at local points, the slot statistics method was applied. The statistics were calculated for samples within slots with a constant width (Shirai et al. 2008). Hence, the resulting practical spatial resolution of the statistics was determined by the slot width applied to each calculation. Throughout the present investigation, the resulting statistics were calculated from more than 2000 samples per slot. The statistics were calculated without using a velocity bias correction scheme from preliminary data analysis. The spatial resolution of the sensor is considered for capturing the spatial structure of the flow in the gap region. In the present study, the velocity profile sensor was mainly used to examine the flow behaviors in the tip clearance region. This was done because the flow was anticipated to be highly three dimensional in this area and hence a high spatial resolution was required. The resulting mean velocities and velocity variances were calculated using slot statistics from the raw measurement data. The slot width set for the statistical calculations was determined to be 100 μm, which was indeed larger than the theoretical spatial resolution of the sensor itself (σ_z=22 μm). The question is whether the slot width was sufficiently small in order to resolve the expected flow structures in the region. To examine this question, the statistics were calculated using different slot widths are calculated. Fig. 8 shows statistics calculated with different slot widths (100, 300, 1600 μm) for the raw data shown in Fig. 7. The results of the LDV measurement were shown together in the same plots for reference. The statistics calculated with a slot width of 1600 μm correspond to the spatial resolution of the LDV in the axial direction. Fig 8(a) clearly indicates that the two velocity peaks captured with the velocity profile sensor using the small slot widths were not captured by the LDV. The large slot width of 1600 μm corresponding to the axial resolution of the LDV also failed to capture the two peaks. A slot width of 300 μm or smaller is required to see the two peaks. For the proper determination of the slot width, one should look at the velocity variance since it clearly shows the contribution of this parameter. This is because the velocity variance varies depending on the slot width size while the contribution of the spatial resolution remains constant regardless of the slot width. Fig. 8(b) shows the velocity variance calculated for different slot widths. Clearly the LDV failed to capture the behavior of the velocity variance because it already failed to trace the behavior of the mean velocity profile (see Fig. 8(a)). The variance value calculated for the results of the velocity profile sensor shows a strong dependence on slot width. The variance calculated for a single location shows larger values for larger slot widths due to the spatial averaging effect. The variance for the slot width of 1600 μm results in excessively large variance values at the locations where the velocity gradient is steep. The variance values calculated with a moderately sized slot width of 300 μm still shows rather high values compared to those calculated with the 100 μm slot width. By decreasing the slot width, the variance profile for a slot width of 100 μm shows little difference compared to that for a 300 μm slot width. However, the profile calculated with the 100 μm slot width starts to show statistical scattering which is most likely due to the relatively small number of samples contained in each slot. Therefore, the slot width of 100 μm should be an appropriate choice for calculating the velocity statistics shown in the present paper without being seriously influenced by the spatial averaging effect.

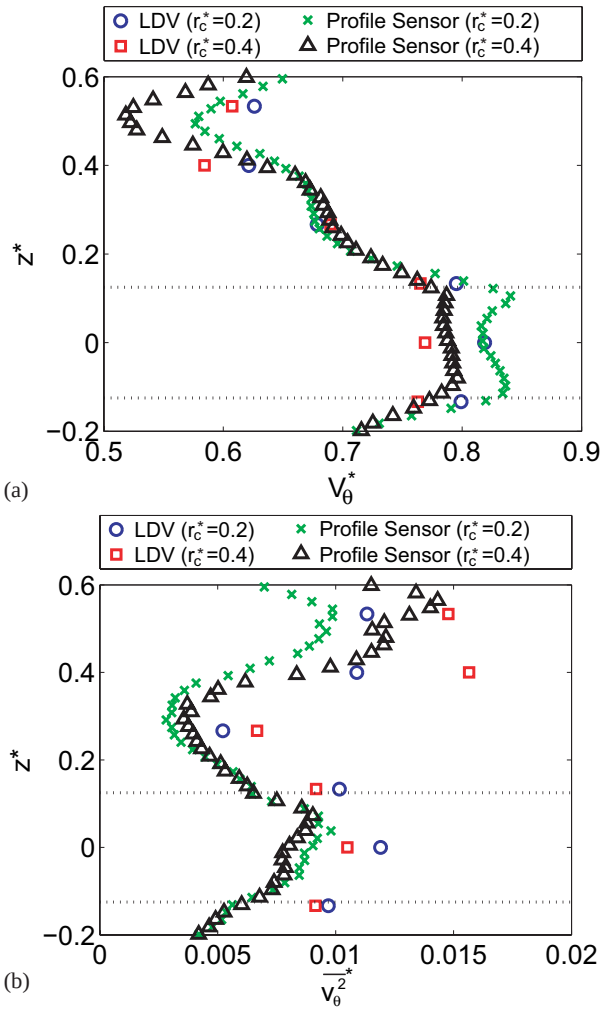

Fig. 9 Comparison of the circumferential velocities measured with the LDV and the velocity profile sensor in case F2: (a) mean velocity $V_\theta{}^*$; (b) variance of fluctuating velocity $\overline{v_\theta{}^2}^*$. The dotted lines indicate the position of the upper and lower surfaces of the disk. The mean velocities (a) measured with the both techniques show good agreement, although the two velocity peaks detected with the velocity profile sensor were not detected with the LDV. The fluctuating velocities (b) clearly always show higher values for the LDV, indicating that the results of the LDV are biased due to the spatial averaging effect.

4 Results

4.1 Comparison between the LDV and the velocity profile sensor

The measurement results obtained with the conventional LDV and the velocity profile sensor are compared. The profiles of the circumferential mean velocity $V_\theta{}^*$ along the axial direction at two different locations $r_c^* = 0.2$ and 0.4 are presented in Fig. 9(a). The variance of the circumferential velocity fluctuation $\overline{v_\theta{}^2}^*$ for these positions is plotted in Fig. 9(b). For the calculation of the statistics, a slot width of 100 μm was applied for the raw results of the velocity profile sensor. The results obtained with the two measurement techniques are in good agreement and the general trends of the flow velocities are well captured at the two different locations. Although the agreement of the mean velocity in the inter-disk region is especially excellent in Fig. 9(a), several discrepancies can be observed. For example, the results of the conventional LDV did not indicate the existence of the two velocity peaks captured with the velocity profile sensor near the edge of the disk surface. The existence of the two velocity peaks has been implied by numerical simulation, e.g., (Al-Shannag et al. 2002), though the experimental evidence is first provided by the present measurement. The velocity minima occurring near the middle of the inter-disk space were not clearly captured by the LDV, while they were captured with the velocity profile sensor. This is attributed to the spatial averaging on the measurements with the LDV. The steep velocity gradient is spatially averaged over the measurement volume and the variance between the fluctuating velocity shows an obvious difference of the results measured with the two techniques. The results obtained with the LDV exhibit consistently larger variance compared with those obtained with the velocity profile sensor. The values of the LDV measurement results are approximately 1.8 times larger than those of the velocity profile sensor. This is again due to the spatial averaging effect. The fluctuating velocity at a given local point is the difference between the instantaneous velocity and the local mean velocity. In the case of the velocity profile sensor, both the local instantaneous velocities and the local mean velocities were measured with a high spatial resolution, and hence the resulting variance of the fluctuating velocities were captured properly within the given spatial resolution. However, in the case of the conventional LDV, the spatially averaged mean velocity was subtracted from the instantaneous velocity and therefore, the resulting variance of the velocity fluctuation produces consistently larger values. The steeper the velocity gradient, the higher the spatial averaging effect on the mean velocity and hence the variance of the fluctuating velocity biases toward larger values. The effect is minimized for the velocity profile sensor because of the calibration of the local fringe spacings which results in a high spatial resolution. In addition, the possible influence of the fringe spacings due to some distortions of the incident laser beams into the enclosure casing is corrected with the in-situ calibration for the measurements with the velocity profile sensor. In conclusion, the spatial resolution of the conventional LDV turned out to be insufficient for the present flow and, therefore, the following discussions are restricted mainly on the results obtained with the velocity profile sensor.

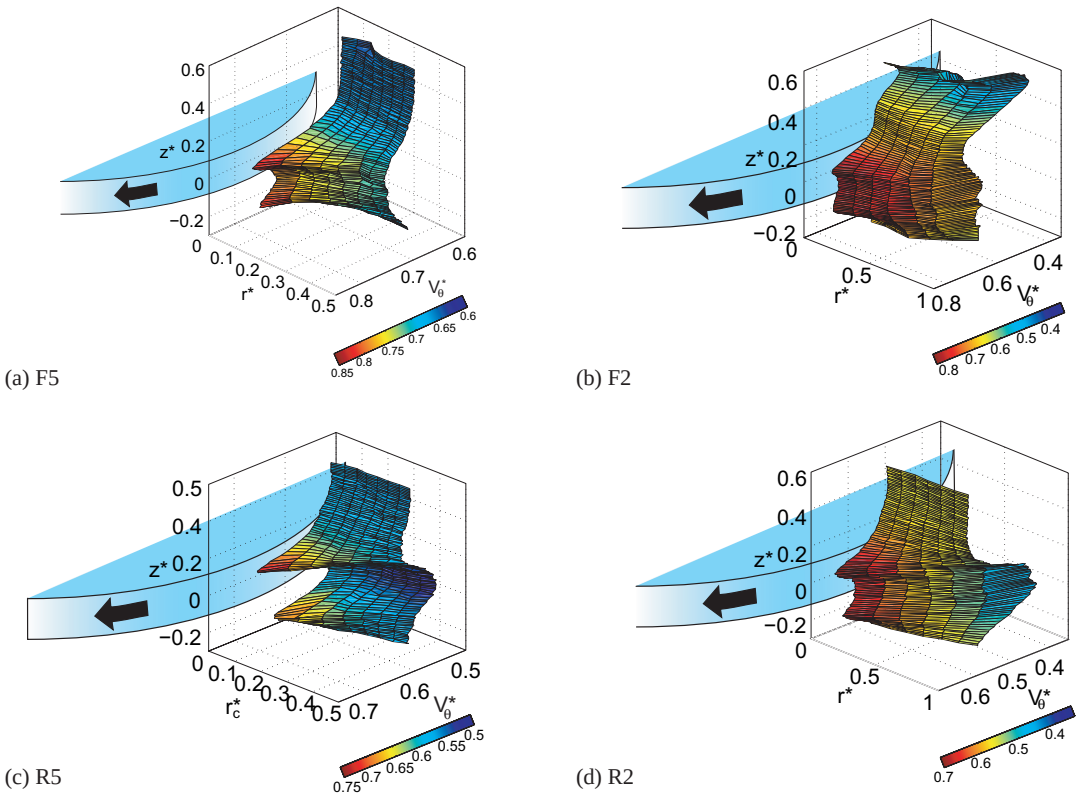

Fig. 10 Three-dimensional contour surface plots of the normalized mean velocity $V_{\theta}{}^{*}$ in the circumferential direction: (a) F5; (b) F2; (c) R5; (d) R2 (see Tab. 1 for the definitions of the conditions). The positions of the two disks are schematically shown together in the respective figures.

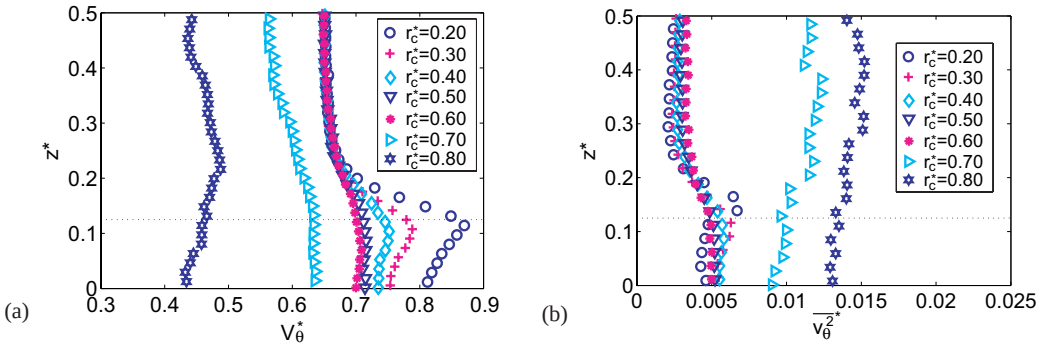

Fig. 11 Normalized velocity profiles along the axial direction for case F5 at different radial locations: (a) mean velocity $V_{\theta}{}^{*}$; (b) variance of fluctuating velocity $\overline{v_{\theta}{}^{2}}^{*}$. (see Fig. 3 for coordinate definition)

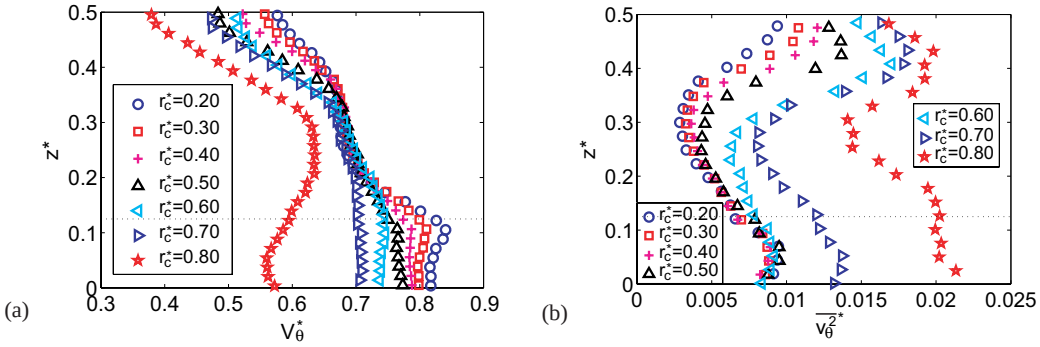

Fig. 12 Normalized velocity profiles along the axial direction for case F2 at different radial locations: (a) mean velocity $V_{\theta}{}^{*}$; (b) variance of fluctuating velocity $\overline{v_{\theta}{}^{2}}^{*}$.

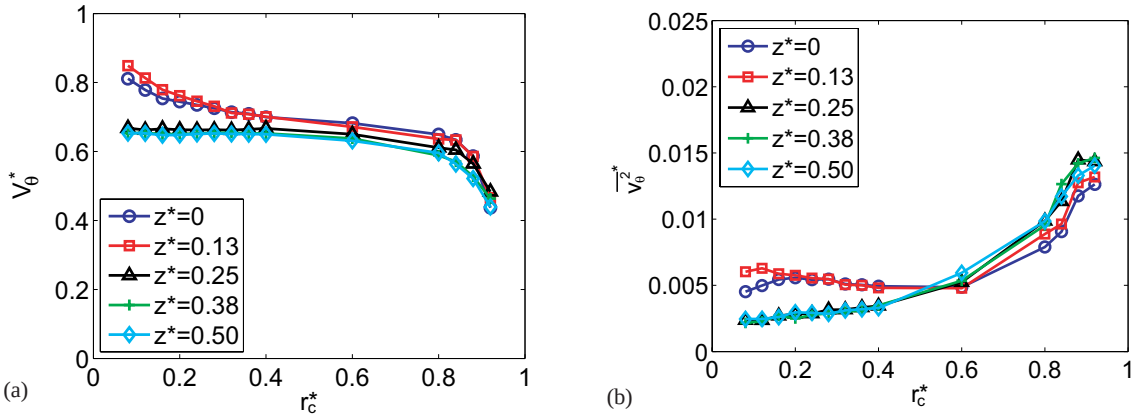

Fig. 13 Normalized velocity profiles along the radial direction for case F5 at different axial positions: (a) mean velocity $V_\theta{}^*$; (b) variance of fluctuating velocity $\overline{v_\theta{}^2}^*$.

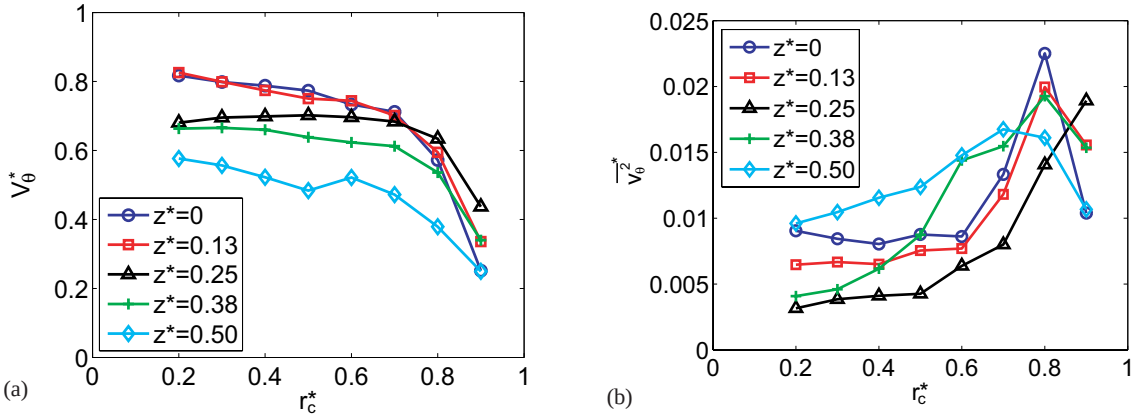

Fig. 14 Normalized velocity profiles in the radial direction for case F2 at different axial locations: (a) mean velocity $V_\theta{}^*$; (b) variance of fluctuating velocity $\overline{v_\theta{}^2}^*$.

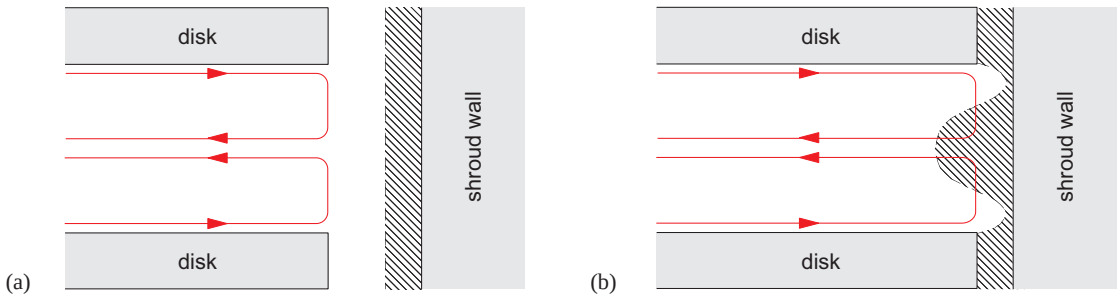

Fig. 15 Sketch of the secondary flow pattern in the boundary layers: (a) case F5; (b) case F2. The shaded area indicates the boundary layer on the shroud.

4.2 General flow regimes in the four cases

The reconstructed normalized distributions of the circumferential mean velocity $V_\theta{}^*$ are shown in Fig. 10 as three-dimensional surface-contour plots for the all four cases. They clearly indicate the existence of the steep velocity gradients in the radial and axial directions. This reflects the anticipated feature of the flow in the gap region – strong mean shears are induced in two directions and they merge near the corner edges of the disk. These four plots also show that the flow exhibits somewhat different behavior depending on the gap width and shroud shape. The two peaks of the mean velocity at the disk edges can be clearly observed in the cases of the 5 mm gap width in Fig. 10(a, c) while the peaks for the cases of the 2 mm gap width are less clearly distinguished in Fig. 10(b, d). The two peaks of the mean ve-

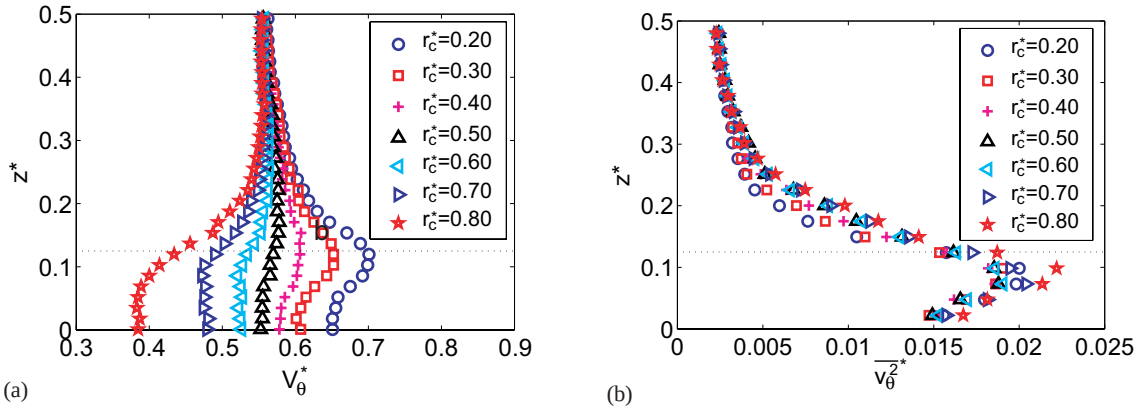

Fig. 16 Normalized velocity profiles along the axial direction for the case R2 at different radial locations: (a) mean velocity $V_\theta{}^*$ and (b) fluctuating velocity $\overline{v_\theta{}^2}^*$.

locity at the disk edges can be clearly observed in the cases of the 5 mm gap width while the peaks for the cases of the 2 mm gap width are less clearly distinguished. Differences in the shroud shape also influence the flow. The mean velocity is smaller in magnitude for the cases involving the ribbed shroud and larger in magnitude for the flat shroud cases. This can be explained by the existence of the large inter-rib region (see Fig. 4). In order to examine the influences of the gap width and the shroud shape, the velocity distributions are compared in greater detail in the following sections.

4.3 Tip clearance

We compare the results of cases F5 and F2 to check the effects of the tip clearance. Figs. 11 and 12 show the normalized distributions of the circumferential velocity $V_\theta{}^*$ along the axial direction at different radial locations for cases F5 and F2, respectively. Both the mean and the variance of the velocity fluctuation are shown in the figures. In these figures, the position of the upper surface (z^*=0.125) is indicated by a dotted line. The mean velocity distributions near the disk tip show a monotonic decrease toward the shroud wall in both cases (see Figs. 11(a) and 12(a)). The velocity behavior in the middle of the disks is remarkably different in the two cases. In case F2, the velocity $V_\theta{}^*$ varies significantly in the axial direction compared to that of case F5. The velocity variance also varies in case of F2, while it remains nearly constant along the axial direction for a given radial location in case F5 (see Figs. 11(b) and 12(b)). The peak in the inter-disk region corresponds to the steep velocity gradient measured in the mean velocity in Fig. 12(a). On the other hand, the location corresponding to that of the other peak in the tip clearance region does not exhibit a steep velocity gradient for the mean velocity. The velocity variance shows a peak at the location with no significant turbulence production in the same velocity component. This feature is not observed in the case of F5 shown in Fig. 11.

The normalized profiles of $V_\theta{}^*$ and $\overline{v_\theta{}^2}^*$ along the radial direction of cases F5 and F2 are shown in Figs. 13 and 14, respectively. In case F5 plotted in Fig. 13, the profiles at three different locations in the inter disk region collapse well into a single curve (z^*=0.25, 0.38 and 0.50), while those in the tip clearance region exhibit boundary-layer-like profiles near the disk tip locations (z^*=0 and 0.13). This boundary-layer-like flow behavior near the shroud wall is mostly the same for the different vertical locations. On the other hand, the normalized velocity distribution for case F2 plotted in Fig. 14 exhibits substantial changes at the different vertical positions. The velocity profiles along the radial direction for case F2 show similar distributions as for case F5 in the tip clearance region (z^*=0 and 0.13), but they are smaller than those in case F5 in the inter disk region (z^*=0.38 and 0.50). The velocity distributions gradually decrease near the middle of the inter disk region in case F2. Hence, the thickness of the boundary layer on the shroud wall should remain constant in the inter disk region in case F5, while it could vary in case F2. The simple illustration to explain this presumption is presented in Fig. 15. When the space between the disk tip and the shroud wall is sufficiently large (see Fig. 15(a)), boundary layers on the disks and the shroud wall do not interfere each other. In contrast, when the tip clearance becomes narrow (see Fig. 15(b)), they start to interfere in the gap region.

4.4 Existence of ribs

The influence of the ribbed shroud is examined. The normalized profiles of the circumferential mean velocity $V_\theta{}^*$ and velocity variance $\overline{v_\theta{}^2}^*$ are shown in Fig. 16 in case R2. Here

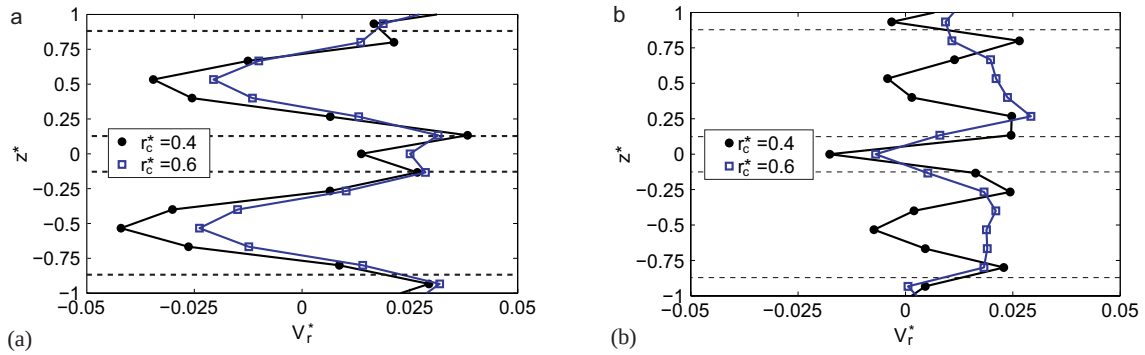

Fig. 17 Normalized radial velocity profiles along the axial direction at two different radial locations for cases (a)F5, (b) R5.

we look on the results of case R2 since overall tendency of the distributions of cases R2 and R5 are quite similar, and the tip clearance of the case R2 is closer to that of a real HDD. The profiles in case R2 in Fig. 16 indicate that the flow behaves in a different manner as compared to those in case F2. The mean velocity gradient observed in the middle of the disks ($0.3 \le z^* \le 0.5$) in case F2 is not observed in the same region for case R2. Concerning the velocity magnitude, the mean velocity in the tip clearance region is smaller than that in case F2. The velocity fluctuation at the inter disk region is substantially smaller in case R2 compared to that in the same region in case F2. The velocity variance profiles at different radial locations exhibit almost identical behaviors in case R2 and they have a peak slightly below the position of the disk upper surface. The axial profiles of the velocity variance decreases toward the inter disk location and they almost asymptotically merge into a single line. On the other hand, the axial profiles of the velocity variance behave differently in case F2. The profiles follow similar trends along the different radial locations, especially in the location near the disk tip $r_c^* \le 0.5$. The profiles show a general increase toward the outer locations, which can be explained by the approach toward the shroud wall surface. Tracing the variation of the velocity variance profiles from the disk middle plane $z^*=0$ toward the inter-disk region $z^*=0.5$, the profiles increase toward a small peak between the disk surface and the disk middle plane.

5 Discussion

The radial velocity component V_r^* was measured with the LDV to examine the existence of the secondary flow structures in the gap region. Fig. 17 shows the mean velocity profile along the axial direction at two different radial locations $r_c^*=0.4$ and 0.6 in cases F5 and R5. As shown in Fig.17(a), V_r^* exhibits peaks with positive values near the disk surfaces and it decreases toward the inter disk region where it eventually exhibits negative peaks. The tendency is nearly the same for the two radial positions, which suggests the existence of the secondary flow in r–z plane in case F5 as schematically depicted in Fig. 15(a). The secondary flow is caused by the boundary layer developing over the disk surface due to the centrifugal force in the radial direction. The region of the boundary layer is referred to as an Ekman layer in the theoretical analysis of the flow by Schuler et al. (1990). On the other hand, V_r^* in case R5, Fig.17(b), shows remarkably different flow pattern as compared with that in case F5. In addition, the velocity profiles at the two radial locations are somewhat different; hence the development of secondary flow is not evident in this case. From the present investigation, clear evidence of the third vortex structure and the complex flow structures was not discernible in the tip gap region. In order to facilitate such discussion, measurement of both circumferential and radial components would be of interest. The measurement of the axial velocity component is also of high interest in order to examine the existence of possible inter-disk momentum exchange through the gap region.

The results of the two different gap widths indicate a significant difference of the flow behavior with respect to the gap width. We suspect that there may be a certain gap width nondimensionalized with the disk thickness at which the flow exhibits different behaviors between the states depicted in Fig. 15. The flow in the conditions of the two gap widths chosen in the present study cannot provide the information of such a *critical* gap width. Furthermore, the flow behavior in the tip gap region with smaller gap widths is of great interest for the development of the next generation of HDDs. Decreasing the size of the gap width seems to be a promising strategy for reducing the flow induced vibration of hard disk drives (Imai et al. 1999; Imai 2001). A similar approach is taken in turbomachinery developments toward increasing efficiency by reducing the leakage of fluid at the tip clearance (Prakash et al. 2006).

6 Conclusions

An experimental investigation of the flow in the tip clearance region of rotating disks and the shroud wall is reported for the first time using laser Doppler techniques. The flow was driven by co-rotating disks in a cylindrical enclosure model to simulate a HDD. Non-intrusive measurements of the circumferential velocity components in the gap region were performed with a conventional LDV and the velocity profile sensor. The main focus of the investigation was on the complex behaviors of the flow in the tip clearance region where past experimental investigations have never focused nor been able to investigate. The velocity measurements were carried out in total for four different experimental configurations with the combination of two different gap widths and shroud shapes with and without ribs. The measurement results of the two techniques showed qualitatively good agreement but the results of the LDV suffered from the spatial averaging effect along the longitudinal axis of the measurement volume. In contrast, the complex flow velocity structures were successfully captured with the velocity profile sensor with a theoretical spatial resolution of about 22 μm. The mean velocity and velocity variance were calculated from highly spatially resolved raw profiles of the circumferential velocity. The resulting velocity statistics revealed the existence of a highly distorted three dimensional boundary layer in the clearance region due to the strong shear forces working in the two orthogonal directions merging at the sharp corner of the disk edge. For the cases of the flat shaped shrouds, the results exhibited significant difference of the velocity behavior around the inter disk region near the shroud surface for the two different gap widths. In the case of the narrow tip clearance, a significant velocity gradient along the vertical direction was observed in the inter disk region. In contrast, the velocity distribution stayed almost uniform in the case of the wider tip clearance. When the the gap width becomes smaller, the boundary layer developing over the disk surface interacts with another boundary layer developed over the shroud wall. The investigation of the flow with the ribbed shroud exhibited different behaviors compared to that with the flat shape shroud. Investigation of the gap flow with a smaller width is a challenging task. The incident laser beams of the sensor are easily reflected or refracted at the disk or shroud surface due to the different media used for the experimental model and the working fluid. Such reflection and refraction makes measurement of the flow velocity inside the gap infeasible. One solution for avoiding the reflection and refraction is to use a model and working fluid with identical refractive indices. Simultaneous measurements of the flow velocities and the disk vibration with non-intrusive techniques are also of interest for future investigations.

Acknowledgements This research was financially supported by the Storage Research Consortium (SRC) and the Deutsche Forschungsgemeinschaft (CZ55/20-2). The support is greatly acknowledged. The research stay of Y. Yaguchi at TU Dresden was supported by the Deutsche Akademische Austauschdienst (DAAD), which is highly appreciated. The authors are grateful to Mr. A. Voigt for setting up the FDM velocity profile sensor, to Mr. M. Neumann for providing a signal processing program, and to Dr. Y. Naka for helping in the preparation of the manuscript.

References

Abrahamson SD, Eason JK, Koga DJ (1989) The flow between shrouded corotating disks. Phys Fluids A 1: 241–251

Al-Shannag M, Herrero J, Humphery JAC, Giralt F (2002) Effect of radial clearance on the flow between corotating disks in fixed cylindrical enclosures. J Fluids Eng 124: 719–727

Bayer C, Shirai K, Büttner L, Czarske J (2008) Measurement of acceleration and multiple velocity components using a laser Doppler velocity profile sensor. Meas Sci Technol 19: 055401 (11 pp)

Budwig R (1994) Refractive index matching methods for liquid flow investigations. Exp Fluids 17: 350-355

Büttner L, Czarske J, Knuppertz H (2005) Laser-Doppler velocity sensor with submicrometer spatial resolution that employs fiber optics and a diffractive lens. Appl Optics 44: 2274–2280

Büttner L, Bayer C, Voigt A, Czarske J, Müller H, Pape N, Strunck V (2008) Precise flow rate measurements of natural gas under high pressure with a laser Doppler velocity profile sensor. Exp Fluids 45: 1103–1115

Czarske J (2001) Laser Doppler velocity profile sensor using a chromatic coding. Meas Sci Technol 12: 52–57

Czarske J, Büttner L, Razik T, Müller H (2002) Boundary layer velocity measurements by a laser Doppler profile sensor with micrometre spatial resolution. Meas Sci Technol 13: 1979–1989

Edwards RV (ed) (1987) Report on the special panel on statistical particle bias problems in laser anemometry. J Fluids Eng 109: 89–93

Fukaya R, Obi S, Masuda S, Tokuyama M (2002) Flow instability and elastic vibration of shrouded corotating disk systems. Exp Fluids 33: 369–373

Humphrey JAC, Gor D (1993) Experimental observations of an unsteady detached shear layer in enclosed corotating disk flow. Phys Fluids A 5: 2438–2442

Imai S, Tokuyama M, Yamaguchi Y (1999) Reduction of disk flutter by decreasing disk-to-shroud spacing. IEEE Trans Magnetics 35: 2301–2303

Imai S (2001) Fluid dynamics mechanism of disk flutter by measuring the pressure between disks. IEEE Trans Magnetics 37: 837–841

Kanagai S, Suzuki J, Obi S, Masuda S (2007) Flow instability and disk vibration of shrouded corotating disk system. J Fluids Eng 129: 1306–1313

Kang N, Raman A (2006) Vibrations and stability of a flexible disk rotating in a gas-filled enclosure–Part 2: Experimental study. J Sound and Vib 296: 676–689

Kirpekar S, Bogy D B (2008) Computing the aeroelasitc disk vibrations in a hard disk drive. J. Fluids and Structures 24: 75–95

König J, Voigt, A, Büttner, L, Czarske J (2010) Precise micro flow rate measurements by a laser Doppler velocity profile sensor with time division multiplexing, Meas Sci Technol (accepted for publication)

Miles P (1996) Geometry of the fringe field formed in the intersection of the two Gaussian beams. Appl Optics 35: 5887–5895

Pang CK, Ong EH, Guo G, Qian H (2008) Experimental dynamic characterizations and modelling of disk vibrations for HDDs. ISA Transactions 47: 85–93

Pfister T, Büttner L, Shirai K, Czarske J (2005) Monochromatic heterodyne fiber-optic profile sensor for spatially resolved velocity measurements using frequency division multiplexing. Appl Optics 44: 2501–2510

Prakash C, Lee CP, Cherry DG, Doughty R, Wadia AR (2006) Analysis of some improved blade tip concepts. J Turbomachinery 128: 639–642

Schuler CA, Usry W, Weber B, Humphrey JAC, Greif R (1990) On the flow in the unobstructed space between shrouded corotating disks. Phys Fluids A 2: 1760–1770

Shirai K, Bayer C, Voigt A, Pfister T, Büttner L, Czarske J (2008) Near-wall measurements of turbulence statistics in a fully developed channel flow with a novel laser Doppler velocity profile sensor. Euro J Mech B/ Fluids 27: 567–578

Suzuki H, Humphrey JAC (1997) Flow past large obstructions between corotating disks in fixed cylindrical enclosures. J Fluids Eng 119: 499–505

Takeda S, Takashi K, Tagawa N, Mori A, Mizoh Y, Nakakita M (2007) Study on flow-induced vibration of head-disk assembly mechanisms in actual hard disk drive. Microsyst Technol 13: 767–775

Tatewaki M, Tsuda N, Maruyama T (2001) An analysis of disk flutter in hard disk drives in aerodynamic simulations. IEEE Trans Magnetics 37: 842–846

Wu S C (2009) A PIV study of co-rotating disks flow in a fixed cylindrical enclosure. Exp Therm Fluid Sci 33: 875–882

Yamamoto Y, Obi S, Masuda S (2004) Effect of disk-shroud spacing on flow induced vibration in corotating disk system. Proc ASME Information Storage and Processing Systems Conference, June 14-16th, 2004, Santa-Clara, CA